

# Computer simulation of Langmuir collapse

A.I. Dyachenko<sup>a</sup>, A.N. Pushkarev<sup>a</sup>, A.M. Rubenchik<sup>b</sup>, R.Z. Sagdeev<sup>c</sup>, V.F. Shvets<sup>a,1</sup>  
and V.E. Zakharov<sup>d</sup>

<sup>a</sup>Scientific Council on Complex Problem "Cybernetics", Academy of Sciences of the USSR, Vavilova 40, 117333 Moscow, USSR

<sup>b</sup>Institute of Automation and Electrometry, Siberian Division of the Academy of Sciences of the USSR,

Universitetsky Prospekt 1, 630 090 Novosibirsk, USSR

<sup>c</sup>Space Research Institute, Academy of Sciences of the USSR, Profsovnaya 84 / 32, 117810 Moscow, USSR

<sup>d</sup>Institute for Theoretical Physics, Academy of Sciences of the USSR, Kosygina 2, 117334 Moscow, USSR

The problem of Langmuir wave collapse in 2D and 3D plasma is considered. A new approach for computer simulation of this phenomenon is proposed, which includes two different theoretical models: averaged dynamical equations and Vlasov's set of equations. It allows to take into account all essential effects during the whole process of collapse and, hence, to get a reliable picture of the collapse in detail and to save markedly computer resources. Peculiarities of the numeric methods are also discussed.

## 1. Introduction. Langmuir collapse in the inertial interval

Langmuir wave collapse predicted theoretically in 1972 [1] and recently confirmed experimentally [2, 3] is of fundamental importance for modern plasma physics. Specifically, collapse – the formation of catastrophically depressed density wells filled by trapped oscillations – is the main collisionless wave energy dissipation mechanism and the natural structural element of strong Langmuir turbulence both in cosmic and laboratory plasmas. For the past one and a half decade the collapse of Langmuir waves has been under intensive analytical and numerical investigations (see reviews [4–7] and references therein; and recent works [8–18]). It should also be noted that since [1] wave collapse became a conventional concept of modern physics, wide range applications have been found in the study of self-focusing for monochromatic waves, collapses of

electromagnetic and lower-hybrid oscillations, and other types of wave collapses [19].

The general scenario for Langmuir collapse is the following: As a result of the development of modulational instability in a turbulent plasma, density cavities filled with Langmuir oscillations are formed. The initial energy density  $W$  in the cavity is of the order of the average turbulent level  $W_0$  and the characteristic size of the cavity  $l_0 \sim r_D \sqrt{nT/W}$  is of the order of the Langmuir wavelength. The process of cavity compression becomes rapidly self-similar and the cavity acquires an universal noticeably flattened shape. During the collapse the energy of the oscillations trapped in the cavity is conserved. In the final stage the wave-particle becomes important and Langmuir oscillations trapped in the cavity are "burned out" through the acceleration of plasma electrons. As a result the energy is transferred to a small group of fast particles. The process of energy burnout is fast and in general its duration does not exceed several hundreds of plasma periods.

Up to the final stage the cavity evolution is described by a set of dynamical equations aver-

<sup>1</sup>Present address: Department of Physics, Auburn University, Auburn, AL 36849-5311, USA

aged over fast time obtained in ref. [1] in the framework of hydrodynamical plasma description:

$$\Delta(2i\dot{\Psi} + 3\omega_p r_D^2 \Delta\Psi) = \frac{\omega_p}{n_0} \nabla \cdot (\delta n \nabla\Psi), \quad (1a)$$

$$(\delta\ddot{n} - c_s^2 \Delta\delta n) = \Delta \frac{|\nabla\Psi|^2}{16\pi M}, \quad (1b)$$

where  $\Psi$  is the averaged electric field  $E = \frac{1}{2}\nabla(\Psi e^{-i\omega_p t} + \text{c.c.})$  potential, and  $\delta n$  is the quasineutral plasma density variation. These equations preserve the integrals of motion, the number of quanta

$$N = \int |\nabla\Psi|^2 d\mathbf{r} \quad (2)$$

and the Hamiltonian

$$H = \int \left( \frac{3r_D^2}{16\pi} |\Delta\Psi|^2 + \frac{\delta n}{16\pi n_0} |\nabla\Psi|^2 + \frac{1}{2} M n_0 v^2 + \frac{M c_s^2}{2n_0} (\delta n)^2 \right) d\mathbf{r}, \quad (3)$$

and have for sufficiently large initial conditions collapsing solutions in 2D and 3D situations. The important properties of Langmuir collapse in the inertial interval follow from system (1) at  $d = 2, 3$ . The negativity of the Hamiltonian is a sufficient condition for collapse, but for  $d = 3$  this condition is exceedingly stronger and collapse takes place for the following initial conditions [4]:

$$H < 0, \quad d = 2, \\ < \frac{3}{16\pi} \left( \frac{r_D}{l_0} \right)^2 N, \quad d = 3, \quad (4)$$

where  $l_0$  is the characteristic size of the initial perturbation.

For sufficiently intensive oscillations  $W/nT > m/M$  one can neglect the fact that the sound velocity in (1b) is finite and the collapse is transformed into the supersonic regime. Asymptotically at  $t \rightarrow t_0$  the supersonic collapse is self-

similar:

$$|E| \sim \frac{f(\xi)}{(t-t_0)^2},$$

$$\frac{\delta n}{n_0} \sim \frac{V(\xi)}{(t-t_0)^{4/d}},$$

$$\xi = \frac{r}{(t-t_0)^{2/d}},$$

$$l \sim (t-t_0)^{2/d}, \quad (5)$$

where  $t_0$  is the singularity formation time and  $l$  the characteristic cavity size.

The collapsing cavity has an asymmetrical oblate shape with the electric field in the cavity center directed along the short size. The cavity asymmetry is connected with the fact that the spherically symmetrical collapse model is non-real: in such a model the field in the cavity center is equal to zero, the ponderomotive forces are absent and the hump density formation in the cavity center takes place. Numerical calculations have demonstrated that a dipole charge distribution in the cavity is a more realistic one. Since 1974 [20] eqs. (1) are repeatedly solved numerically (see works presented in ref. [3] and also in refs. [9, 15]). The calculated results well confirmed the cavity properties described above and, in particular, have demonstrated the sufficiently arbitrary initial condition for the self-similar regime (5).

The applicability of system (1) is restricted to small hf (high frequency) energy levels  $W/nT \ll 1$  and large cavity sizes  $kr_D \ll 1$ . As the cavity collapses and the field intensity grows, the set of effects which are not taken into account become important.

Among them we mention first of all the interaction between electrons and Langmuir oscillations. Also electron nonlinearities, nonlinearity saturation dispersion law change; hydrodynamical ion nonlinearities and others can play an important role. Simultaneous and adequate taking into account of these effects in the frame of some "improved" dynamic equations system seems to

be impossible. Of course the investigation of some effects inserted in model (1) in numerical experiments (the model Landau damping [9, 15], the electron nonlinearities in the quasi-one dimensional approximation [14], nonlinearity saturation and ion kinetics [16]) are of substantial interest. An adequate general physical picture description in the final stage of collapse is possible, however, only by using the full kinetic equation system:

$$\begin{aligned} \frac{\partial f_e}{\partial t} + v \cdot \frac{\partial f_e}{\partial r} + \frac{e}{m} \nabla \varphi \cdot \frac{\partial f_e}{\partial v} &= 0, \\ \frac{\partial f_i}{\partial t} + v \cdot \frac{\partial f_i}{\partial r} - \frac{e}{M} \nabla \varphi \cdot \frac{\partial f_i}{\partial v} &= 0, \\ \Delta \varphi &= -4\pi e \int (f_i - f_e) dv. \end{aligned} \quad (6)$$

Namely the relatively short final stage of the Langmuir cavity collapse, during which the oscillation energy transformation to electrons takes place, is of main practical and scientific interest. Therefore the numerical simulation of the final collapse stage, which can take into account the main nonlinear and kinetic effects from “first principles”, is of principal importance, i.e. the solution of the kinetic equations (6) by the particle method [21–25]. Only such simulations can answer the principal questions for an adequate building-up of the turbulence theory about the anisotropy degree and sizes of the cavity in the final stage of evolution, the time of cavity burning out, the energy part which is transformed to electrons, the accelerated particle distribution and its anisotropy, and investigate the most important cavity characteristics during and after its burning out.

This paper presents a survey of works of several authors [13, 16–18, 21, 22] which are devoted to this extremely difficult problem. The huge computational need for doing multidimensional kinetic calculations forced us to maximally take into account a priori properties of the collapsing cavity in the formulation of the numerical experiment and the agreement of the numerical model applied both with the physical problem specifica-

tion and the peculiarities of the multiprocessor computer system used for calculations, ES-1037–ES-2706 SRI, Academy of Sciences of the USSR. Below, these questions are discussed in detail. Particularly, the Langmuir collapse concept “through simulation” is proposed; in this framework the solution of the self-similar dynamic equations (1) is used as an initial condition for the system (6). The detailed 2D picture of collapse is obtained for a wide inertial interval, and the different cavity evolution regimes have been investigated. Three-dimensional kinetic calculations have demonstrated a clear picture of the collapse. The cavity parameters, the density variation amplitude and the maximal oscillation energy were found to be substantially different from the 2D case. Also the electron acceleration character differed from the one obtained in the 2D case

## 2. The difficulties and general principles of the simulation of Langmuir collapse

First of all we estimated the computational need for the simulation of the cavity evolution. Achievement in the numerical model of a sufficiently large inertial interval  $l_0/l_{\min} \gg 1$  for the self-similar solution formation before additional mechanisms switch on, which are not inserted in (1), is of principal importance. We set for a crude estimation  $l_0 \sim 50l_{\min}$ ,  $l_{\min} \leq 20r_D$  [2, 3, 16–18]. Using the estimate for the collapse development time [4]

$$t_k \omega_p \sim \left( \frac{MnT}{mW} \right)^{1/2},$$

we obtain

$$t_k \omega_p \sim 10^3 \sqrt{M/m}.$$

For such an evolution time the  $d$ -dimensional cavity evolution problem must be considered in the region  $\sim (10^3 r_D)^d$ . The particle number used

for such a region is  $N \sim 10^{3d} N_D$  ( $N_D \gg 1$ , the total number of electrons and ions in the volume  $r_D^d$ ) and the number of time steps is  $\sim 10^3 \sqrt{M/m} (\omega_p \Delta t)^{-1} = 5 \times 10^3 \sqrt{M/m}$  (we have used the typical particle model value  $\Delta t = 0.2 \omega_p^{-1}$ ). Introducing the characteristic  $\tau$  (time in microseconds to advance on one particle time-step) of the standard particle method for the total simulation time we obtain (in s)

$$T = 5 \times 10^{3d-3} \sqrt{M/m} N_D \tau. \quad (7)$$

Substituting for a crude estimation  $\tau = 40 \mu\text{s}$ ,  $N_D = 50$  we obtain that even in the 2D case for the model mass ratio  $M/m = 100$  it takes tens of thousands of computer time hours for the calculation of one variant. Hence the pure kinetic simulation in a wide inertial interval is absolutely unacceptable.

It is clear, however, that the computational process can be naturally divided into two parts. At the beginning the averaged equations (1) are solved on the whole inertial length. After that the obtained self-similar solution is used as the initial condition for the kinetic simulation by the particle method. We proposed to call this approach the ‘‘through simulation’’ and have realized it in refs. [13, 16] (we also used this approach later for a 1D Langmuir turbulence simulation [26]). The transition moment  $t^*$  from averaged to kinetic description must be defined by the averaged description conditions:

$$kr_D \ll 1, \quad \frac{W_{\max}}{nT} \leq 1, \quad \frac{\delta n}{n_0} \ll 1 \quad (8)$$

near the bound of their applicability. As our calculations have shown, the compression down to  $l \sim 30r_D$  and the maximum hf energy density levels up to  $W_{\max}/n_0 T \sim 0.2$  are acceptable. Because the kinetic calculations consume the main part of the computer time, it is clear that the ‘‘through simulation’’ technique provides huge (about several orders) computational gain

Consider the transition from dynamic to kinetic description in detail. As the initial data of the particle method are the ion and electron distribution functions  $f_i(\mathbf{r}, t)$  and  $f_e(\mathbf{r}, t)$  in phase space it is necessary to reconstruct them from the complex high-frequency potential envelope  $\psi(\mathbf{r}, t)$  and the low-frequency plasma density variation  $\delta n(\mathbf{r}, t)$ . In agreement with the applicability conditions of the set (1) at the moment of transition to the kinetic description the particle distribution was assumed to be Maxwellian:

$$f_\alpha = \frac{n_\alpha(\mathbf{r})}{2\pi V_{T_\alpha}^2} \exp\left[-\left(\frac{|V - V_\alpha(\mathbf{r})|^2}{2V_{T_\alpha}^2}\right)\right], \quad \alpha = i, e. \quad (9)$$

Because of their large mass, the ions participate only in the low-frequency motions.  $n_i = n_0 + \delta n$ , where  $\delta n$  is determined from eq. (1b). The macroscopic ion velocity  $V_i$  is searched from the linearized continuity equation  $\partial \delta n / \partial t + n_0 \operatorname{div} V_i = 0$ . The electrons participate in both low- and high-frequency motions:  $n_e = n_0 + \delta n + \delta \tilde{n}$ . The hf density variation component and the electron velocity are determined from Poisson and linearized electron motion equations:

$$\Delta \varphi = 4\pi e \delta \tilde{n}, \quad \frac{\partial V_e}{\partial t} + 3V_{T_e}^2 \nabla \frac{\delta \tilde{n}}{n_0} = \frac{e}{m} \nabla \varphi,$$

where

$$\varphi = -\left[\frac{1}{2} \Psi(\mathbf{r}, t^*) \exp(-i\omega_p t^*) + \text{c.c.}\right].$$

It should be pointed out that two-stage practical realization ‘‘through simulation’’ requires independent particle simulation of the final stage of the collapse. In spite of the fact that the whole investigation implies, of course, the ‘‘through simulation’’ performance, such a statement is undoubtedly of independent interest especially when the ‘‘through’’ realization is impossible for some reasons or too complicated. Namely in such a way the kinetic simulation of the Langmuir collapse by the particle method has begun [8,

27–30]. However, in these works the statement of the numerical experiment did not correspond with the physics of the investigated phenomenon in an optimal way because of a strong deficiency of computer resources. Insufficient account of physical and geometrical cavity properties has led to nonadequateness and/or vagueness of the simulation of the general collapse picture as a whole. Note several considerable points:

(1) The optimum choice of the initial conditions is extremely important. From (3) it follows that for  $\delta n = 0$ ,  $H > 0$ , i.e. the uniform initial distribution choice leads in the 2D case to violation of the sufficient collapse condition (4), and in the 3D case to its near-boundary character when the influence of nonphysical effects of the model is essential. As a rule in this case the initial uniform distribution is broken into localized cavities [27–29]. Therefore the effectiveness of the “computational volume” used sharply drops.

It is clear that the choice of the initial conditions for the pure kinetic problem is rather arbitrary. In any case, however, the initial plasma state must contain small ion and charge density perturbations  $\delta n < 0$  and  $\rho = -e \delta \tilde{n}$  (to imitate the density well filled by hf oscillations) which obey the inertial interval description conditions (8) and sufficient collapse conditions (4).

(2) The small model particle mass ratio (for example,  $M/m \leq 25$  [27–29]) understates artificially the ion inertia role, which is rather essential for the final collapse stage and leads to inertial interval shortening.

(3) The periodic boundary conditions used [8, 27–30] are rather inefficient from the computational resources viewpoint and (if the special measures for zero harmonic generation are not taken) physically ungrounded in the case of one cavity in the considered region. In this case because of a nonzero potential jump along the small axis of the dipole cavity nonphysical cavities–satellites birth is unavoidable. This effect disturbs the characteristics and unadmissibly reduces the main cavity description under the condition of deficiency of resources.

A physically correct and rather effective approach for cavity evolution simulation is proposed and realized in refs. [13, 16–18]. This approach uses the cavity properties described above in the maximum degree. Suppose that the dipole cavity is flattened along the  $z$ -axis. Hence the electric field potential is asymmetric along the dipole axis and symmetric in the perpendicular direction:

$$\begin{aligned} \varphi(\mathbf{r}_\perp, z) &= \varphi(-\mathbf{r}_\perp, z) = -\varphi(\mathbf{r}_\perp, -z) \\ &= \varphi(x, -y, z) = \varphi(-x, y, z). \end{aligned} \quad (10)$$

The question of cavity symmetry was discussed for example in ref. [4] and this symmetry was demonstrated in numerical studies. Breaking of symmetry in ref [15] was associated with the special case of rotating cavities. The symmetry properties allow us to use only a part of the cavity. For the simulation of a  $d$ -dimensional cavity by the particle method it is enough to carry out the calculations in the region

$$\begin{aligned} 0 \leq \mathbf{r}_\perp \leq L_\perp, \quad -\frac{1}{2}L_z \leq z \leq \frac{1}{2}L_z, \\ \left. \frac{\partial \varphi}{\partial \mathbf{n}} \right|_r = \left. \frac{\partial n_{1,e}}{\partial \mathbf{n}} \right|_r = 0, \end{aligned} \quad (11)$$

which contains  $1/2^{d-1}$  part of the cavity. One can reach a larger computational gain by solving the averaged equations (1) in the region  $0 \leq \mathbf{r}_\perp \leq L_\perp$ ,  $0 \leq z \leq L_z/2$ , containing  $1/2^d$  part of the cavity with boundary conditions  $\Psi|_{z=0} = 0$ , is sufficient. Unfortunately, in the particle method there are no analogous conditions for particles, the electron cross the  $z = 0$  plane and the kinetic description must be carried out in the region (11) with the boundary conditions for reflecting particles.

Because the minimum periodical cell contains two whole cavities with the electric field directed in opposite directions, the statement described above leads to a drop in the computational resources consumption of  $2^{d+1}$  for averaged equations simulation and of  $2^d$  for particle simulation

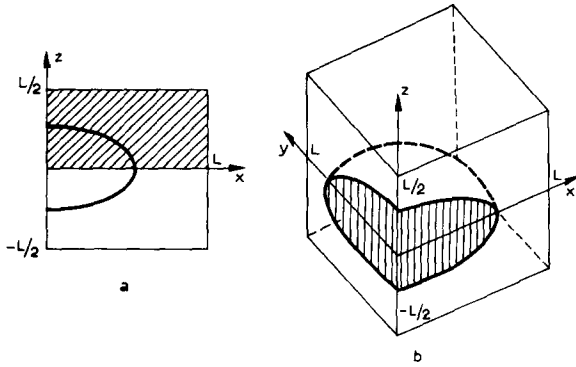


Fig 1 The kinetic simulation region containing  $1/2^{d-1}$  part of the cavity, (a)  $d = 2$  (shaded region is sufficient for solving averaged equations), (b)  $d = 3$

with respect to the problem with equivalent periodical boundary conditions with zero averaged electric field.

The optimal ratio between linear region sizes is defined by the cavity anisotropy, which is time-dependent and can become both more and less than the initial one. It is reasonable therefore to put  $L_{\perp} = L_z = L$ , which corresponds to an anisotropy of the order of 2. Approximately such a value was observed in calculations [13, 15–18] and in laboratory experiments [2]. In accordance with this fact it is advisable to carry out the kinetic calculations in the region  $0 \leq r_{\perp} \leq L$ ,  $-\frac{1}{2}L \leq z \leq \frac{1}{2}L$  containing  $1/2^{d-1}$  part of the cavity (see fig. 1) with boundary conditions for reflecting particles and zero normal field component.

Similarly, for the solution of the averaged equations in the first stage of the “through simulation”, it is reasonable to carry out the calculations in the region containing  $1/2^d$  part of the cavity,  $0 \leq r_{\perp} \leq L_0$ ,  $0 \leq z \leq \frac{1}{2}L_0$ , with the boundary conditions

$$\left. \frac{\partial \Psi}{\partial \mathbf{n}} \right|_{\Gamma_1} = \Psi|_{z=0} = \left. \frac{\partial \delta n}{\partial \mathbf{n}} \right|_{\Gamma} = 0,$$

where  $\Gamma_1$  is the part of the boundary without the points  $z = 0$ .

It should be noted that during the simulation of the collapse in the frame of (1) our method of “cutting-out” [13, 16] seems to be rather efficient. It means, in fact, that the sizes of the calculation region follow the diminished cavity sizes. Practically, we extracted the central part of the calculation region  $0 \leq r_{\perp} \leq \frac{1}{2}L$ ,  $0 \leq z \leq \frac{1}{4}L$  in discrete time moments corresponding to the hf energy density growth by an order of ten (here  $L$  is the variable region size which varies in cutting-out time moments). The required functions in the cutted-out region were reconstructed with the help of cubical splines. The number of grid-points during the cutting-out process was constant; the control was performed with the help of motion integrals (2), (3). So, the cutting-out method leads to an increase of the inertial interval without additional consumption of computational resources.

Let us now discuss the question about the simulation of the final stage of the collapse by the particle method with the help of the principles described above [21, 22]. The spatial grid which is necessary for the calculation of charges and fields is introduced by dividing the plasma volume  $L^d$  into regular cells each of linear size  $\Delta$ , which defines the spatial resolution in the system, the cell number in each direction  $M = L/\Delta$  is chosen generally as  $M = 2^p$  ( $p$  is an integer number) for the applicability of FFT algorithms which are used for the calculation of forces acting on the particles.

The whole database volume  $V = Q + V_g$ ,  $Q \gg V_g$  is divided by particle arrays each of  $Q = 8dN_D M^d (\Delta/r_D)^d$  bytes (every particle is described by  $2d$  parameters – coordinates in phase space) and the common grid arrays of volume  $V_g$  containing several arrays of volume  $V_0 = (M+1)^d$  (depending on the dimensionality and calculation details [21]). It was taken into account here that the grid functions in the statement (10), (11) are real (i.e. expanded into sine and cosine products contrary to complex exponents in the case of the periodical problem); the spatial grid nodes are placed not in the cell centers but in their apexes

(in the periodical problem  $V_0 = jM^d$ , where  $j = 1$  for real and  $j = 2$  for complex arrays).

Using the estimates  $M = 128$ ,  $\Delta = r_D$ ,  $N_D = 50$  one can obtain that for the 2D problem  $V \approx Q \sim 13$  Mbytes. It is clear that such database volumes cannot be placed in RAM computer storage and have to be placed in external memory units (magnetic disks, as a rule). In addition a large calculation volume requires the use of a computer with a large integral performance. This means both high calculation speed and fast access to information on the magnetic disks (MD). From this viewpoint the multiprocessor system (MPS) is quite acceptable. The MPS consists of the HOST ES-1037 and several loosely coupled array processors (AP) ES-2706. The MPS is organized in SRI, Academy of Sciences of the USSR jointly with the specialists of the Bulgarian Academy of Sciences and IZOT (see, for example, ref [21]). The maximum AP performance is 12 Mflops and it has memory page organization with a total memory volume of Mbyte (each memory page contains  $2^{16}$  words). The MPS permits independent calculations in HOST and AP and data I/O. This parallelism allows us to carry out simultaneous calculations in AP and I/O between HOST and AP, HOST and MD.

Consider the calculation process for the single AP case. The phase "picture" as a whole (the particle parameters) is placed on the MD. The grid arrays and also two memory buffers for the particle I/O are placed in the AP memory. The total particle set is divided in equal portions, each of memory buffer size. Each portion is read successively from MD, put to AP and is written to MD after processing. The memory buffers are

organized by the "handshake" principle, i.e. during the processing of the  $n$ th particle portion in the first memory buffer, the output of the  $(n - 1)$ th portion from the second memory buffer and after that the input of the  $(n + 1)$ th portion are performed. After that the buffers change places. In the HOST computer also two memory regions, each of the AP memory size, are reserved. The particle I/O between HOST and MD is also organized by the "handshake" principle: in one time step the reading is performed from one region and the writing is performed to another one. In the next time step the regions change places (see table 1). Such memory organization provides the existence of one undamaged phase picture in the case of hardware malfunction. It is easy to see that the processing time of one portion of particles is defined by the longest process time, i.e. either I/O time or AP processing time. Because the I/O speed  $U_0$  is constant ( $U_0 \sim 1$  Mbyte/s) it defines the largest possible particle processing rate. It is easy to obtain that the time which is required for the I/O of one particle in the  $d$ -dimensional case is of the order of  $16d \mu\text{s}$  (every particle is described by  $2d$  numbers each of 4 Mbyte to be read and write). Therefore the processing time for one particle cannot be greater than  $16d \mu\text{s}$ . Such a hard condition was fulfilled by carefully programming the movement and change distribution subroutine using Array Processor assembler Language. Finally, one should note that an additional gain can be reached at the cost of parallelizing calculations and I/O data flow into several MD-AP chains controlled by a single HOST computer [21]

Table 1

The temporal diagram of parallel processes in MPS. The number of developed particles is given in parentheses. G and P are the input and output of particle parameters in and out of AP, W and R are the reading and writing of particle parameters from and to MD.

AP running	$(n - 1)$	$(n)$	$(n + 1)$
I/O AP $\leftrightarrow$ Host	G( $n - 2$ )P( $n$ )	G( $n - 1$ )P( $n + 1$ )	G( $n$ )P( $n + 2$ )
I/O Host $\leftrightarrow$ MD	W( $n - 3$ )R( $n + 1$ )	W( $n - 2$ )R( $n + 2$ )	W( $n - 1$ )R( $n + 3$ )

### 3. The formulation of the 2D problem specification and the simulation

The 2D geometry is the minimum one for Langmuir collapse. It is natural therefore that the final collapse stage investigation is based mostly on 2D statements [8, 13, 16, 27, 29, 30] But the 2D situation is rather specific: it is a borderline one, i.e. even taking into account the average description (1) of small terms of different physical nature (nonlinearity saturation, dispersion law change and so on) can stop the collapse. It is clear that this effect is especially strong for near-threshold cavities.

Consider the properties of the quasistationary cavitons formed because of stopping of collapse. We shall consider only the nonlinearity saturation effect. Close to the stationary state, the low-frequency motions can be considered as adiabatic ones and the electron distribution function can be taken in the Boltzmann approximation. Assuming for the sake of simplicity that the ion temperature is zero, we have

$$\delta n = n_0 [\exp(-\Phi/T) - 1]. \quad (12)$$

Here  $\Phi$  is the ponderomotive force potential:

$$\Phi = e^2 |E|^2 / 4m\omega_p^2.$$

Expanding the exponent and substituting (12) into (1a) we get in dimensionless variables

$$\Delta(\Psi + \Delta\Psi) + \nabla \cdot [\nabla\Psi \cdot (|\nabla\Psi|^2 - |\nabla\Psi|^4)] = 0 \quad (13)$$

The time is here normalized by  $\omega_p^{-1}$ , the spatial dimensions by  $(3/2)^{1/2} r_D$  and the electric field by  $(32\pi n_0 T)^{1/2}$ .

Eq. (13) is a Hamiltonian one:

$$i\Delta\Psi_t = -\frac{\Delta H}{\delta\Psi^*},$$

$$H = \int [|\nabla\Psi|^2 - \frac{1}{2}|\nabla\Psi|^4 + \frac{1}{3}|\nabla\Psi|^6] d\mathbf{r}. \quad (14)$$

Its stationary solution of the form

$$\Psi = \exp(i\lambda^2 t) \varphi$$

is described by the equation

$$-\lambda^2 \Delta\varphi + \Delta^2\varphi + \nabla \cdot [\nabla\varphi |\nabla\varphi|^2 (1 - |\nabla\varphi|^2)] = 0, \quad (15)$$

where  $\lambda^2$  is the nonlinear frequency shift in the caviton ( $\lambda$  is its characteristic reciprocal size). These solutions realize a minimum of  $H$  for a fixed number of waves in the caviton  $N = \int |\nabla\varphi|^2 d\mathbf{r}$ . Multiplying (15) by  $\Psi^*$  and integrating we get

$$\lambda^2 N + \int (|\nabla\Psi|^2 - |\nabla\Psi|^4 + |\nabla\Psi|^6) d\mathbf{r} = 0 \quad (16)$$

Consider the scale transformation conserving  $N$  in the 2D case  $\varphi \rightarrow \varphi(\lambda\mathbf{r})$ . In this case

$$H(\lambda) = \int [\lambda^2 (|\nabla\Psi|^2 - \frac{1}{2}|\nabla\Psi|^4) + \frac{1}{3}\lambda^4 |\nabla\Psi|^6] d\mathbf{r}. \quad (17)$$

In the caviton  $H(\lambda)$  has to reach a maximum. Hence  $\partial H / \partial \lambda^2 |_{\lambda^2=1} = 0$  for localized stationary solutions. This gives

$$H + \frac{1}{3} \int |\nabla\varphi|^6 d\mathbf{r} = 0. \quad (18)$$

It is well known that if we neglect the nonlinearity saturation the caviton size  $\lambda^{-1}$  is arbitrary. This is clear, e.g., from the fact that after the substitution  $\mathbf{r} \rightarrow \lambda\mathbf{r}$  the stationary equation which describes the caviton neglecting the nonlinearity saturation,

$$-\Delta\varphi_0 + \Delta^2\varphi_0 + \nabla \cdot (\nabla\varphi_0 |\nabla\varphi_0|^2) = 0, \quad (19)$$

is independent of  $\lambda$ .

It is clear from (18) that  $H$  is zero for such solutions while the caviton energy

$$\omega_p N = \omega_p \int |\nabla\varphi_0|^2 d\mathbf{r} = \omega_p N^{\text{th}}$$

is also independent of its size. If the initial caviton energy is larger than the critical value  $\omega_p N^{\text{th}}$ , the caviton collapses.

Including the saturation lifts the degeneracy and the caviton equilibrium size is determined uniquely by its energy. We define this connection assuming that the nonlinearity saturation is small. We look for a solution of the form

$$\varphi = \varphi_0 + \delta\varphi, \quad \delta\varphi \ll \varphi_0,$$

where  $\varphi(\mathbf{r})$  is the solution of (19). One can assume that the function  $\varphi$  is real. Introduce  $\delta N = N - N^{\text{th}} = 2 \int (\nabla\varphi_0, \nabla\delta\varphi) d\mathbf{r}$ . Linearizing eqs. (16) and (19) we get

$$\lambda^2 = \frac{3(N - N^{\text{th}})}{2 \int |\nabla\varphi_0|^6 d\mathbf{r}}. \quad (20)$$

We see that if the energy enclosed in the caviton is considerably larger than the critical one,  $N \geq N^{\text{th}}$ , the equilibrium caviton size in dimensional variables is of the order of the Debye radius. It is clear that such cavitons cannot exist due to Landau damping. If we are just above criticality, the caviton size increases,

$$l \sim r_D \sqrt{N^{\text{th}} / (N - N^{\text{th}})}, \quad (21)$$

and the role of Landau damping decreases rapidly.

We have already mentioned that as the caviton size decreases, many effects neglected in (1) become important. We mention only electron nonlinearities with characteristic time  $\tau^{-1} \sim (kr_D)^2 \omega_p E^2 / 8\pi nT$ , corrections to the dispersion law with  $\tau^{-1} \sim (kr_D)^4 \omega_p$  and the nonlinearity saturation with  $\tau^{-1} \sim \omega_p (E^2 / 8\pi nT)^2$ . Since for the caviton  $(kr_D)^2 \sim E^2 / 8\pi nT$ , all these effects must be considered at the same time. Therefore, the calculations given above are only quantitative and show that the caviton structure formation can be expected only in the regime just above criticality. However, the final conclusion about caviton existence can be drawn only by numerical simulation

In the 2D case we have realized the whole collapse investigation program – the “through simulation” [13, 16]. In the inertial interval the cavity compression is described well by the equation set (1). After transformations to dimensionless variables,

$$|\nabla\Psi|^2 \rightarrow \frac{64\pi}{3} n_0 T_e \frac{M}{m} |\nabla\Psi|^2,$$

$$r \rightarrow \frac{3}{2} r_D \sqrt{\frac{M}{m}} r,$$

$$t \rightarrow \frac{3}{2} \frac{M}{m} \omega_p^{-1} t,$$

$$\delta n \rightarrow \frac{4}{3} n_0 \frac{m}{M} n,$$

these equations take the form

$$\Delta(\dot{\Psi} + \Delta\Psi) = \nabla \cdot (n\nabla\Psi),$$

$$n - \Delta n = \Delta|\nabla\Psi|^2 \quad (22)$$

with corresponding Hamiltonian

$$H = \int [|\Delta\Psi|^2 + n|\nabla\Psi|^2 + \frac{1}{2}n^2 + \frac{1}{2}(\nabla\Phi)^2] d\mathbf{r},$$

where  $\Phi$  is the hydrodynamical low-frequency motion potential  $\partial n / \partial t = -\Delta\Phi$ . In accordance with section 2 the system (22) was solved in the region  $0 \leq x \leq L_0$ ,  $0 \leq z \leq L_0/2$  (see fig. 1a) with the following boundary conditions:

$$\Psi_x|_{x=0} = \Psi_x|_{x=L_0} = \Psi_z|_{z=L_0/2} = \Psi|_{z=0} = \frac{\partial n}{\partial n}|_r = 0.$$

We choose as an initial condition for the set (22) the function  $\Psi$  such that

$$\Delta\Psi = \rho_0 \sin kz (1 + \cos kx), \quad k = \pi/L_0 \quad (23)$$

and for low-frequency plasma density variations

$$\frac{\delta n}{n_0} \Big|_{t=0} = \frac{|\nabla\Psi|^2}{16\pi n_0 T_e}, \quad \delta n = 0. \quad (24)$$

The 2D collapse initial condition  $H < 0$  for the initial distribution (23), (24) takes the form

$$\rho_0 > \rho_0^{\text{th}} = \left( \frac{\pi}{L_0} \right)^2 \left( \frac{384}{181} \right)^{1/2} = \frac{14.4}{L_0^2}$$

with the number of quanta  $N(\rho_0^{\text{th}}) = 2\pi^2/3$

The equation set (22) was solved with the help of FFT algorithms using a technique analogous to that of ref. [31]. The reliability of the calculations was checked by the motion integrals  $N$ ,  $H$ . The initial region size was  $L_0 = 512r_D$ . During the calculation process twofold successive cutting-out was performed and the kinetic simulation was carried out in the region  $L = 128r_D$ . The first simulation stage was finished when the characteristic cavity size was decreased down to  $(20-30)r_D$  or the field energy density in the cavity center was increased up to  $W_{\text{max}}/nT \sim 0.2$ . Further, one of the most important particle methods (the dipole expansion method) was used [21, 25]. We used values standard for such a model  $a = \Delta = r_D$  ( $a$  is the macroparticle half-width) with Gaussian macroparticle charge distribution. The number of model particles of each kind in the Debye cell was changed from 16 to 64; the total number of particles reached  $\sim 8 \times 10^5$ . The simulation adequateness was checked in different ways: by checking the total energy conservation in the field-particles system, the particle number and time-step variation ( $0.2 \leq \omega_p \Delta t \leq 0.4$ ) for the same physical variants, with the help of test calculations for periodic boundary conditions in the region containing two whole cavities with oppositely directed electric fields.

The organization of the kinetic stage of the calculations was performed according to the scheme described in section 2. In the 2D situation the use of one AP with its memory containing grid arrays of the charge density, the forces and their derivatives happened to be sufficient. The volume of one portion of particle which is transferred along the MD-AP chain is equal to 11264 particles. The AP processing time did not exceed the I/O one, i.e. 32  $\mu$ s.

Before presenting the calculation results and their analysis we shall return to the question about the possibility of the appearance of caviton structures. To study them we have performed two additional calculation sets in other, simpler models. In the first of them the calculations were performed in the framework of eqs. (13). In the second one we considered a mixed description [13, 16]. The high-frequency motions were described by the equation

$$\Delta(2i\Psi + 3\omega_p r_D^2 \Delta\Psi) = \frac{\omega_p}{n_0} \nabla \cdot (\delta n_1 \nabla\Psi), \quad (25)$$

and the ion motion in the low-frequency potential  $\varphi$  field was described by the kinetic equation

$$\frac{\partial f_1}{\partial t} + \mathbf{v} \cdot \frac{\partial f_1}{\partial \mathbf{r}} - \frac{e}{M} \nabla\varphi \cdot \frac{\partial f_1}{\partial \mathbf{v}} = 0 \quad (26)$$

and solved by the particle method. The electron distribution, on the other hand, was assumed to be a Boltzmann distribution,

$$\delta n_e = n_0 \left[ \exp\left(-\frac{e\varphi - \Phi}{T_e}\right) - 1 \right] = \delta n_1, \\ \Phi = \frac{e^2 |\nabla\Psi|^2}{4\pi\omega_p^2}, \quad (27)$$

and the charge separation in the lf motions was neglected.

In the static limit this hybrid semi-kinetic description is reduced to eq (13), but besides the nonlinearity saturation effect it describes the ion nonlinearities and the Landau damping on the ions.

#### 4. The results of 2D collapse simulation

As was mentioned above, one of the features of the Langmuir collapse "through simulation" is the presence of a large inertial interval. This enables us to assume that the final collapse stage is independent of the initial electric field and

density distributions in the cavity but is determined solely by the number  $N$  (or energy  $W$ ) of plasmons trapped in it. The threshold value  $N^{\text{th}}$  ( $W^{\text{th}}$ ) can be determined reasonably in the 2D geometry from the condition that the Hamiltonian of the equation set (1) is equal to zero. It is clear that the cavity evolution character has to be defined by the overcriticality parameter  $\epsilon = W/W^{\text{th}} = (\rho_0/\rho_0^{\text{th}})^2$

We shall turn now to the results obtained in the numerical experiments and their analysis. It should be noted first that in the dynamical equation framework the cavities reach rather rapidly the self-similar compression regime (5). This fact was checked by the depression and electric field amplitude changing rate. The largest inertial interval length was reached for variants with two central cavity parts cutting-out. The cavity size up to the moment of transition to the kinetic stage was decreased by a factor of 10 to 15 with respect to its initial size.

After the transition to the kinetic description both particle and averaged simulations were performed. We show in fig. 2 the temporal evolution of the oscillations of the energy density for variant  $\epsilon = 6.6$ . It is clear that dynamical equations satisfactorily describe the collapse up to the oscillation level  $W_{\text{max}} \sim 0.4 n_0 T$ .

The calculations showed, as was expected, that the cavity evolution depends significantly on the initial overcriticality  $\epsilon$ . The calculations were performed for various ion to electron mass ratios,  $100 \leq M/m \leq 1836$ . It was found that for all  $\epsilon$

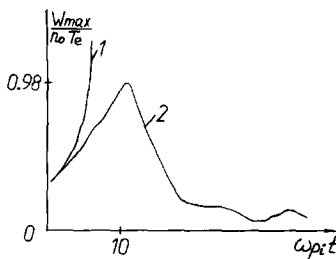


Fig. 2 The dependence of the maximum energy density of the field in the cavity (1) results of the dynamical equations solution, (2) the results of the "through" simulation

the cavity evolution depends on the ion mass in a self-similar way while all characteristic times depend only on the product  $\omega_p t = \tau$

For overcriticality  $\epsilon \geq 6$  a clear collapse picture (see figs. 2–4) was observed. The oscillation energy evolution for several typical variants is shown in fig. 3. It is clear that for  $\epsilon = 6.6$  fast (during  $\tau \sim 7$ ) burning out of an appreciable part of the energy (65%) trapped in the cavity is observed. The spatial electric field energy and plasma density distributions are presented in fig. 4 at several successive moments. The maximum energy density for this variant was  $W_{\text{max}}/nT = 0.98$  and the ion well depth was  $\delta n/n_0 = -0.38$ . It is also seen from fig. 4 that the cavity continues to deepen also after burning-out of Langmuir oscillations due to ion inertia. The cavity size for maximum deepening time is rather large,  $\sim (10 \times 25)r_D^2$ . The electron velocity distribution is also anisotropic (see fig. 5). It is clearly seen that as a result of the collapse the hf field energy is transferred to a relatively small part of the fast electrons, which is accelerated mainly in the direction of the average cavity field (along  $z$ -axis).

For small overcriticalities a long-lived ( $\tau \sim 40$ ) cavity structure was found (see figs. 6, 7). We shall note first its nonstationary nature. Such behavior is completely natural in the framework of eq. (13). Indeed, for the cavity solution the

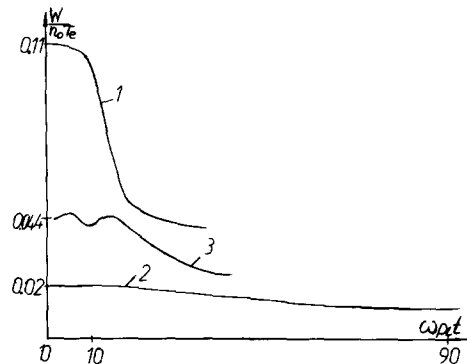


Fig. 3 Time dependence of the average energy density of the field in the cavity (1)  $\epsilon = 6.6$ , (2)  $\epsilon = 1.25$ , (3)  $\epsilon = 2.7$

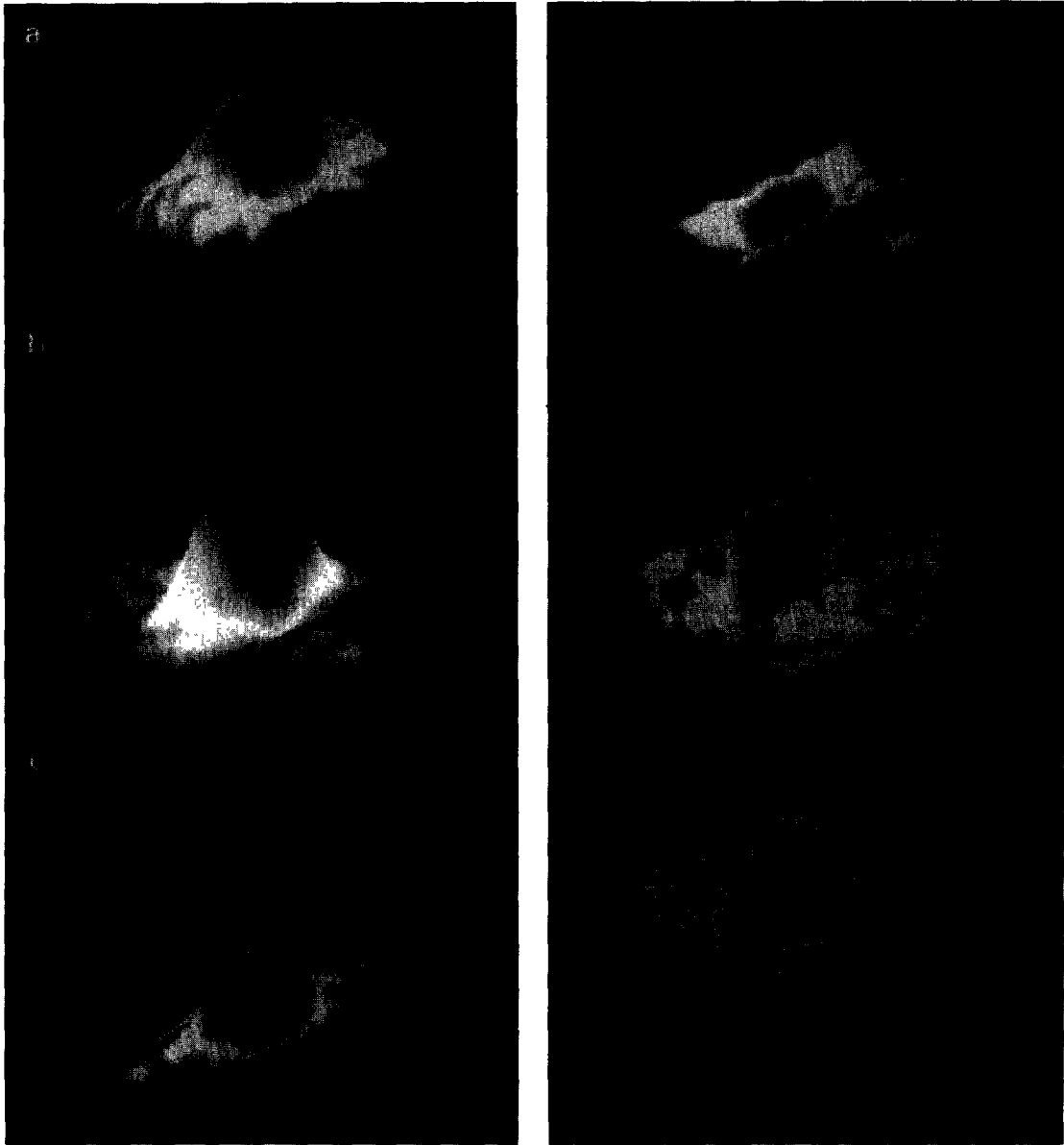


Fig. 4. Spatial distribution of hf field energy  $E^2/16\pi n_0 T_e$  (left) and plasma density  $n_1/n_0$  (right) for the variant with  $\epsilon = 6.6$ , (a) at  $t = 0$ , (b) at the time when the field in the cavity is a maximum ( $t = 10.8\omega_{pe}^{-1}$ ); (c) at the time when the depth of the cavity is a maximum ( $t = 17.2\omega_{pe}^{-1}$ )

Hamiltonian has a completely definite value differing from the initial one. Therefore, because of conservation of the Hamiltonian, the caviton solution can be reached only if small dissipative processes or energy emission beyond the simulation region limits are taken into account

We have performed additional calculations of caviton structures in the framework of (13) and a hybrid semi-kinetic approach (25)–(27). The calculations in these models gave similar results. However, in this case the caviton size turned out to be one-and-a-half to two times smaller than in

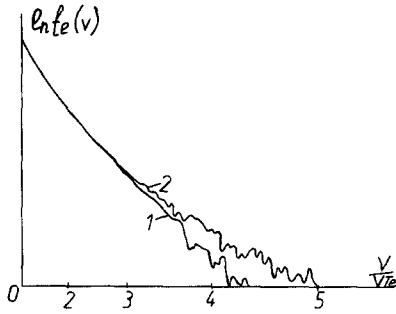


Fig 5 The electron distribution function for the variant  $\epsilon = 6.6$ , integrated over space and the velocities  $V_x$  (1) and  $V_z$  (2) at  $t = 35 \omega_{pe}^{-1}$

the “through simulation”. This fact indicates that such effects as electron nonlinearities, changes in the dispersion law of Langmuir waves and Landau damping make an appreciable contribution to the caviton formation.

We shall now discuss the cause of the caviton damping after the time  $\tau \sim 40$ . Passing through the caviton of size  $l$  the electron gains an energy  $\Delta E = e \int E V dt$ . The electric field  $E$  changes proportionally to  $\cos \omega_p t$ . If the time for passing through the caviton is less than  $\pi/\omega_p$ , the electric field does not change sign and the electron gains an energy  $eEl \sim T$ . Assuming that the characteristic electron velocities are of the order of  $3V_T$  we find that the caviton starts to be strongly damped when  $l = l_{min} \sim 3\pi V_T/\omega_p \sim 10r_D$ , which corresponds to the minimum cavity size obtained in the calculations. When  $l > l_{min}$  the quantity  $\Delta E$  is exponentially small,  $\Delta E \sim T \exp(-l/l_{min})$ , but for our calculations completely finite. Ultimately this nonadiabatic interaction with the electrons leads to the caviton damping.

To check this assumption we performed a one-dimensional calculation by the particle method in which we used as initial condition the soliton solution of the average dynamical equations. It turned out that a soliton with dimensions close to the caviton dimensions obtained in the “through simulation” also burns up after a time of the order of  $\tau \sim 40$ .

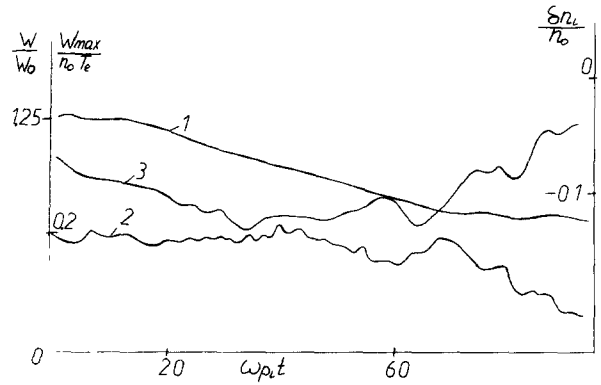


Fig 6 The temporal dependence of the cavity characteristics for the caviton variant  $\epsilon = 1.25$ , (1) average density of the hf field energy  $W/n_0 T_e$ , (2) maximum energy density  $W/n_0 T_e$ , (3) density variation  $\delta n/n_0$

We have described two opposite situations: pure collapse and formation of quasistationary structures. Calculations for moderate overcriticalities,  $2 < \epsilon < 6$ , showed that, as one should expect, in that case an intermediate regime is realized which can naturally be called a delayed collapse (fig. 8). We note that in all cases the minimum caviton size was  $\sim (10 \times 25)r_D^2$ .

So, the 2D “through simulation” has shown that if the initial oscillation energy in the cavity is appreciably larger than the threshold  $N^{th}$ , there occurs in the final stage of the collapse burning out of almost all the energy trapped in the cavity. The minimum cavity size is rather large and is of the order of  $10r_D$ . In this case one can expect that 2D calculations simulate adequately 3D turbulence. If  $N$  is close to  $N^{th}$  then in the final stage a long-lived quasistationary state is formed. Its formation is connected with the 2D nature of the calculations and this result cannot in general be extrapolated to the 3D situation. The results obtained indicate additional difficulties arising in the 2D strong turbulence calculations (see refs. [32, 33]). It is interesting, in particular, to clear the question about the amount of energy captured by the cavity when it is formed as a result of development of modulational instability

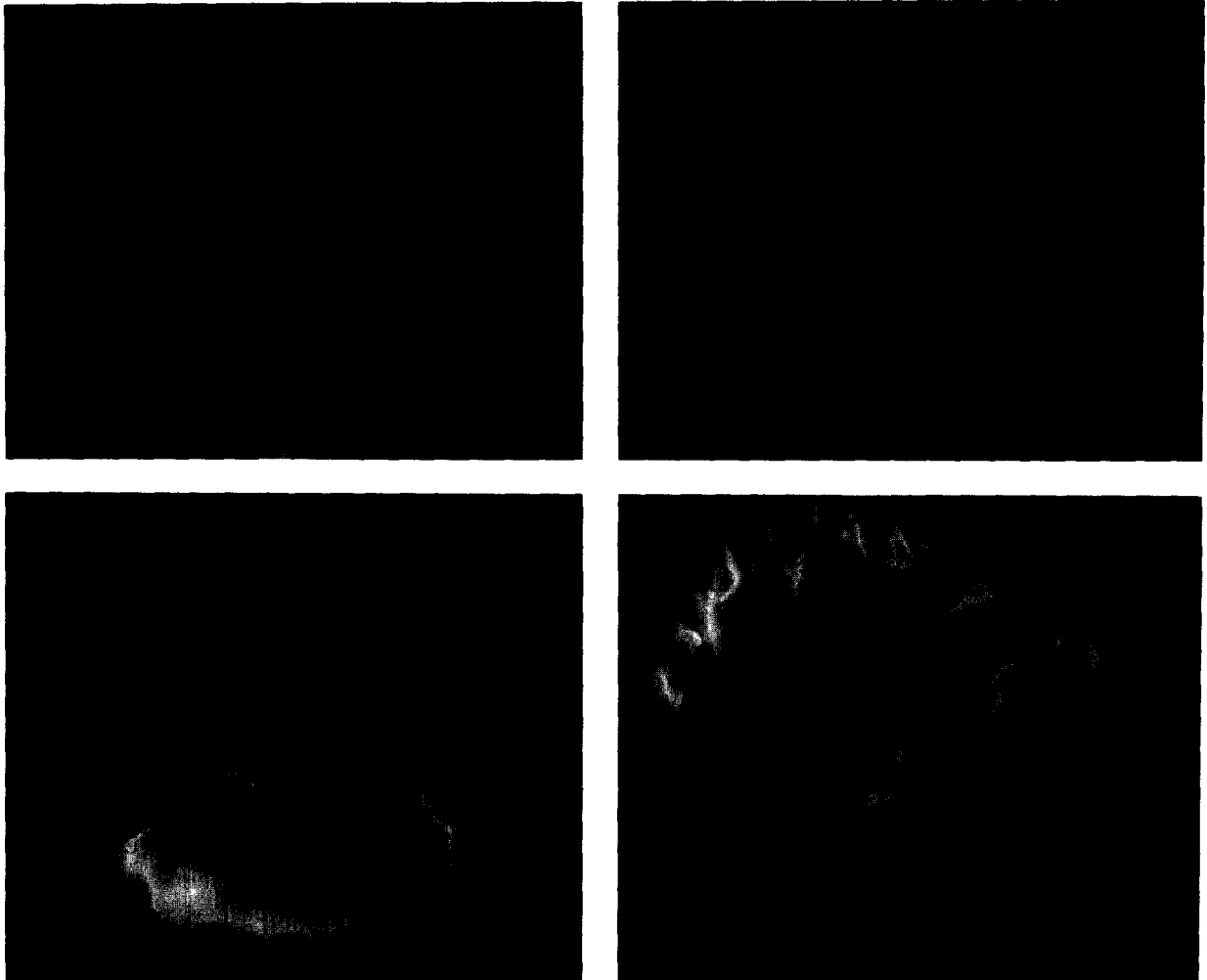


Fig 7 Spatial distributions of the hf field energy  $E^2/16\pi n_0 T_e$  (left) and the plasma density  $n_1/n_0$  (right) for the cavity variant corresponding to  $\epsilon = 1.25$  (two cavities are presented)

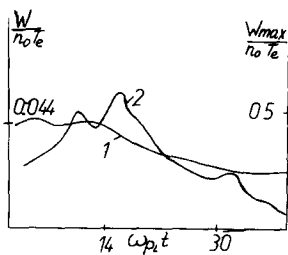


Fig 8 Temporal dependences of the average (1) and the maximum (2) hf field energy in the cavity for  $\epsilon = 2.7$ , corresponding to a delayed collapse

The 2D collapse simulation is much simpler than the 3D one and consideration of the 2D collapse is the natural first step for the investigation of the collapse problem. As was already mentioned above the 2D situation is a specific one and has its own distinctive features. We shall enumerate the most appreciable differences between 2D and 3D collapse:

- (1) From eq. (5) it follows that the hf energy level increases in the 3D case more rapidly than characteristic wave number values of trapped oscillations and can exceed appreciably the thermal

density energy in the evolution process. This fact was demonstrated, for example, in the framework of the calculations of averaged equations [9]. The large density intensity values can lead to a change in wave-particle interaction, electron acceleration character and the energy part transforming them.

(2) It was previously shown that for 2D near-threshold cavities the collapse is stopped and formation of quasistationary structures is typical. In the 3D situation this phenomenon must be absent.

(3) From eqs. (1) and (5) it follows that the ratio of the kinetic energy of the ions,  $\frac{1}{2}n_0V_1^2$ , to the potential one,  $c_s^2n_0(\delta n/n_0)^2$ , varies as  $\sim(t_0 - t)^{4/d-2}$ . Therefore for the 3D case the ion kinetic energy grows faster than the potential one and the density profile in the cavity is defined by the ion inertia but not by the thermal motion. Therefore even though additional nonlinear mechanisms of the final stage would stop the collapse the ion inertia have to compress the cavity down to switching on of electron-oscillation interaction. In this case the density well will continue to deepen even after the burning out of the plasma energy part. Thus, in 3D cavities the plasma variation value must be appreciably larger than in 2D case.

The discussion above illustrates obviously the fact that solution of the 3D problem is of principal importance. In the next sections the final stage of the 3D cavity evolution is investigated by the particle method [17, 18]. Such simulation is near the limits of today's computer capability [21, 22].

## 5. The 3D kinetic model and its realization

We succeeded in solving the problem of the 3D Langmuir cavity evolution using the principles of collapse simulation by the particle method presented in section 2. The huge computational need for the 3D simulation required a very deep insight in cavity properties in the numerical model

[22] and also in the application of parallel computation with its new organization elements [21].

The total astronomical calculation time is of the order of

$$T \sim \frac{2Qt_f}{U_0 m \Delta t}, \quad (28)$$

where  $m$  is the number of processors (not large, as a rule),  $t_f$  the characteristic time for the final stage of the collapse,  $t_f \omega_p \sim 200$ . From (28) taking into account the expressions for  $Q$  and characteristic values  $U_0$  and  $\Delta t$  presented in section 2, it follows that a reasonable maximum calculation time (15–20 h) is reached for a number of cells in each direction of  $M \leq 32$ . Because  $T$  is proportional to  $M^3$  it is difficult to use more grids by means of enlargement of  $m$  or  $\Delta t$ . For  $M = 32$  and the typical particle model value  $\Delta = r_D$  the cavity quarter was simulated in a region  $(32r_D)^3$ , i.e. the whole cavity in a region  $64 \times 64 \times 32r_D^3$ . It is clear that for a sufficiently large inertial interval providing acceleration of heavy ions an increase of the linear size  $L$  is required. It can be performed only at the cost of a more crude grid used with a linear mesh-size exceeding the standard value  $r_D$ . The principal possibility of such inertial interval increase is provided by a sufficiently large minimum cavity size observed in the 2D calculation (see section 4) and laboratory experiments [2, 3] ( $l_{\min} \sim 10-20r_D$ ). The increase of mesh-size  $\Delta$  leads, however, to enhancement of the aliasing effect and a correction of the model becomes unavoidable. Let us consider this question in detail.

For the traditional dipole method with Gaussian particle charge space distribution  $\sim \exp(-r^2/2a^2)$  the long-wave Langmuir oscillation dispersion is

$$\omega(k) = \omega_p \left[ 1 + \frac{3}{2}(kr_D)^2 - \frac{1}{2}(ka)^2 \right] \quad (29)$$

and can differ markedly from the real one. In particular if the particle size  $a > \sqrt{3}r_D$ , the dispersion agent becomes negative. A trial 3D col-

lapse simulation with mesh-size  $\Delta = 2r_D$  and traditional smoothing  $a = r_D$  has demonstrated the strong energy nonconservation due to aliasing effects. The energy conservation was much better in the strong short-wave harmonic suppression ( $a = 2r_D$ ) case. But in this case the dispersion term, however, becomes negative and the collapse is absent. For the long-wave region minimization of dispersion correction and aliasing effects we have chosen the “plateau-like” distribution (for  $n \rightarrow \infty$ )

$$S(k) = \exp[-(ka)^n], \quad (30)$$

which differs from the traditional Gaussian charge distribution. The “plateau-like” distribution makes the spectrum equal to zero at  $k > 1/a$ . The choice of  $a$  and  $n$  was verified by means of a much less expensive 2D model. The correctness of the 2D simulation with the smoothing factor (30) for  $\Delta = 2r_D$  was verified by comparing it with the results obtained for  $\Delta = r_D$ . The test calculations were found to be the best for  $a = 1.4r_D$  and  $n = 6$  (energy nonconservation  $\sim 0.2\%$  during the time  $\sim 300\omega_p^{-1}$ ). One can see that at such smoothing parameters the dispersion of the long-wave part of the spectrum is defined by

$$\omega(k) = \omega_p \left[ 1 + \frac{3}{2} (kr_D)^2 \right],$$

with an accuracy of the order of  $k^4$ . The above expression coincides with the real dispersion of Langmuir waves.

The conclusion about the possibility of using an analogous  $k$ -space smoothing for the 3D case is based on the theoretical prediction about stronger collapse character in the 3D case. This means, at least, that energy flow along  $k$ -space scales is absorbed by plasma particles within a smoothing zone defined from 2D calculations.

The described procedure of standard dipole particle method correction enables to use both linear sizes  $L = 34r_D$  and  $L = 64r_D$ . The last one corresponds to consideration of the whole cavity in the region  $128 \times 128 \times 64r_D^3$ .

The initial conditions for the final collapse stage were chosen in accordance with the requirements described in section 2. To minimize the aliasing effects and to increase the inertial interval we have chosen the initial charge distribution in the cavity as a combination of the eigenfunctions of the boundary problem

$$\begin{aligned} \Delta\varphi = 0, \quad \frac{\partial\varphi}{\partial n} \Big|_r = 0, \\ 0 \leq x, y \leq L, \quad -L/2 \leq z \leq L/2 \end{aligned}$$

for minimum wave number  $k = \pi/L$ :

$$\rho(\mathbf{r}) = \rho_0(1 + \cos kx)(1 + \cos ky) \sin kz.$$

The plasma density variation  $\delta n$  was defined from kinetic and hf pressures balance,

$$\begin{aligned} \frac{\delta n}{n_0} \Big|_{t=0} = -\frac{|E|^2}{16\pi n_0 T_e} + C, \\ C = \frac{1}{16\pi n_0 T_e L^3} \int |E|^2 d\mathbf{r}, \end{aligned}$$

where the constant  $C$  corresponds to zero mean density, which is unavoidable in particle models. The initial particle velocity distribution was chosen to be Maxwellian, the ion temperature and velocity equal to zero.

For the described initial plasma conditions the calculation of integrals (2) and (3) gives in dimensionless variables

$$\begin{aligned} N = \frac{19}{6\pi} \rho_0^2 L^2, \\ H = \left( \frac{\rho_0}{4} \right)^2 \left[ 13.5 - 747 \left( \frac{\rho_0}{32\pi^2} \right)^2 L^4 \right]. \end{aligned} \quad (31)$$

Here  $N$  and  $H$  are normalized by the whole thermal energy  $L^3 n_0 T_e$ , the charge density  $\rho_0$  and length  $L$  by  $en_0$  and  $r_D$ , respectively. Now substituting  $l_0 = L/2$  in the sufficient collapse condition (4) for the initial perturbation amplitude (here the condition  $W/n_0 T \ll 1$  is taken into

account) we have

$$35.9/L^2 = \rho_0^{\text{th}} < \rho_0 \ll 4.99/L. \quad (32)$$

From this condition, in particular, it follows that  $L \gg 7.2$

The particle mass ratio in the calculations was chosen sufficiently large,  $100 \leq M/m \leq 400$ . The total particle number was  $\sim 1.8 \times 10^6$ . The calculation correctness was checked by controlling total energy conservation in the system. The nonconservation did not exceed several percents. Furthermore, in the initial cavity evolution stage (for small long-wave oscillations levels) we always had exact conservation of the integral  $N$ , i.e. the whole field energy

Now consider briefly the peculiarities of 3D software development and realization. The maximum particle processing rate is achieved by grid arrays displacement in the AP main data memory. It should be noted that these arrays cannot be placed in the same memory pages as processing particles because of memory conflicts in the case of simultaneous memory region requirement by the processing program and I/O channel. The number of grid arrays (each of volume  $V_0 = (M+1)^3$ ) is for the 3D case equal to 10: G (the charge density and its Fourier components), FX, FY, FZ (the forces and their Fourier-components), FXX, FXY, FXZ, FYZ, FYY, FZZ (the force derivatives). However, the existence of a sufficient time-stock (the processing time is less than the I/O time) makes possible the calculation of derivatives immediately in the inner cycle and storing only four data arrays. The trial calculations have shown that this problem is solvable if the above memory distribution requirements have been fulfilled. Such data volume can be placed on three AP pages. It means, however, that two array elements have to be placed on different memory pages and results in additional inner cycle programming difficulties, which increase the processing time. From the other side, to minimize the initialization time for I/O between HOST and AP, MD and HOST and AP running, one

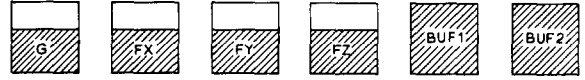


Fig. 9 The grid array distribution in the AP memory for 3D simulation. BUF1 and BUF2 are the memory regions for pumping portions of particles

should use the maximum portion size. Taking into account all previously mentioned circumstances we used in 3D kinetic calculations eight-page AP with a memory distribution presented schematically in fig. 9

The organization of the calculations for the case with one AP coincides with the one described in section 2. In the case of  $m$  AP there are  $m$  MD-HOST-AP chains. Each AP memory distribution remains the same; the phase space on MD is divided by  $m$  parts (each one is intended for the arbitrary AP); the HOST memory contains  $2m$  particle buffers. The whole data processing flow consists of parallel working pipelines. This process becomes possible by means of I/O synchronization between  $m$  MD and the first group of  $m$  HOST memory buffers simultaneously with an analogous I/O process between  $m$  AP and the second group of  $m$  HOST memory buffers. After the particle processing the whole charge density is defined by the summation  $G = \sum_{i=1}^m G_i$ . This process consists of sending each array  $G_i$  from the  $i$ th AP to the others  $m-1$  AP and simultaneous computation of the sum  $G$  in each of the  $m$  AP. This addition does not worsen the time characteristics because it is performed simultaneously with the next I/O. When the calculation of  $G$  has completed the calculation of forces is performed for each of the  $m$  AP. It is easy to show that any other calculation procedure of forces (for example, accumulation of the density array  $G$  in one AP and its subsequent sending to the other ones) is much more expensive.

The described computational procedure provides  $\approx m(1+\alpha)/(1+am)$  times computational gain [21] where  $\alpha \ll 1$  characterizes the relative calculation time for the calculation of the forces using the density. The configuration of the used

multiprocessor system allowed to use in our calculations two AP. The volume of each portion travelling along each MD–HOST–AP chain was equal to 10922 particles. The particle processing time does not exceed the I/O time of 48  $\mu$ s. The average computer system performance per particle turned out to be slightly larger and for one AP equal to 51  $\mu$ s due to some expense; for  $m = 2$  this value was found to be 27  $\mu$ s. The whole database volume on MD was  $2Q \approx 85$  Mbytes.

Finishing this section we shall note that an assembly of methods described here (the using of asymmetry, the doubling of the mesh-size with correction of smoothing, the calculations parallelization) allowed to reach in the 3D case two orders of computational gain with respect to the traditional approach and to perform 3D kinetic cavity evolution simulation.

## 6. The final stage of 3D Langmuir collapse

Consider the results of the numerical experiments. We shall note first of all that in any simulation variant the hf field energy maximum corresponds to the ion density well and coincides with their initial location (the coordinate reference point). The trial calculation set carried out for region size  $L = 32r_D$  has demonstrated the collapse picture: a growth of a hf oscillation intensity maximum of 2 times accompanied by a ion well deepening of 1.5 times. The small inertial interval due to the small initial perturbation led, however, to a fast average hf oscillation energy damping by electrons because of switching on of Landau damping. An appreciable advance was obtained using doubled region size. We have found experimentally the initial perturbation density threshold  $\rho_0^* = 0.009$ , which happened to be the same as calculated from estimation (32),  $\rho_0^{\text{th}} = 0.0088$ . For values  $\rho_0 > \rho_0^*$  the picture of field focusing at the initial density perturbation center and ion well depression was observed, which led

to hf oscillation energy burning out (the spatial physical cavity characteristics for one of the typical variants are given in fig. 10). The choice of the perturbation amplitude  $\rho_0 < \rho_0^*$  led to destruction of the initial field and density amplitude. Similar to the 2D case, we introduced overcriticality parameter  $\epsilon = W(\rho_0)/W(\rho_0^*) = (\rho_0/\rho_0^*)^2$ . The calculation results for an initial hf oscillation energy density in the cavity center of  $0.135 \leq W_{\text{max}}/n_0T_e \leq 0.485$  is presented below; the average hf field energy was changed in the limits  $0.024 \leq W/n_0T_e \leq 0.080$ .

The temporal dependences of the mean hf oscillation energy  $W/n_0T_e$ , the maximum hf oscillation energy  $W_{\text{max}}/n_0T_e$  and the ion well depression  $(n_{\text{max}} - n_{\text{min}})/n_0$  for four simulation variants are presented in fig. 11. For large exceedings  $\rho_0 = 0.02$ ,  $\epsilon = 5$ ,  $M/m = 100$  (variant 1 in fig. 11) and  $\rho_0 = 0.015$ ,  $\epsilon = 3$ ,  $M/m = 100$  (variant 2 in fig. 11) a bright collapse picture with a six times energy growth up to a maximum  $W_{\text{max}}/n_0T_e \sim 3$ , a 3–5 times ion well depression down to  $(n_{\text{max}} - n_{\text{min}})/n_0 \sim 0.7$  and a significant part (70%) of the hf dissipation during  $\sim (8-9)\omega_{p_i}^{-1}$  was observed. In the 2D case for exceedings  $2 < \epsilon < 6$  a “prolonged” collapse was realized (fig. 8) but a “bright” collapse was only for  $\epsilon > 6$ . Even for the regime practically near threshold  $\rho_0 = 0.01$ ,  $\epsilon = 1.1$ ,  $M/m = 100$  (variant 4 in fig. 11) we observed a three-times field energy growth and a 2.3 times well depression during  $\sim 30\omega_{p_i}^{-1}$ . The average oscillations level remained practically unchanged. In the 2D case we have already seen that for the exceeding  $\epsilon = 1.25$  during the same time the cavity structure formation took place (see fig. 6).

To clear the ion inertia role we have carried out twice calculations for the amplitude  $\rho_0 = 0.015$ : for  $M/m = 100$  and  $M/m = 400$  (variants 2 and 3 in fig. 12 respectively). This ion time-scaled variant (see fig. 13) is seen to be the same with respect to a time-shift of  $\sim 4\omega_{p_i}^{-1} - 5\omega_{p_i}^{-1}$  because of the ion immobility at the initial time; the burning-out time in  $\omega_{p_i}^{-1}$  units does not depend on the mass ratio  $\sqrt{M/m}$ . In accordance with the qualitative presentations of the ion iner-

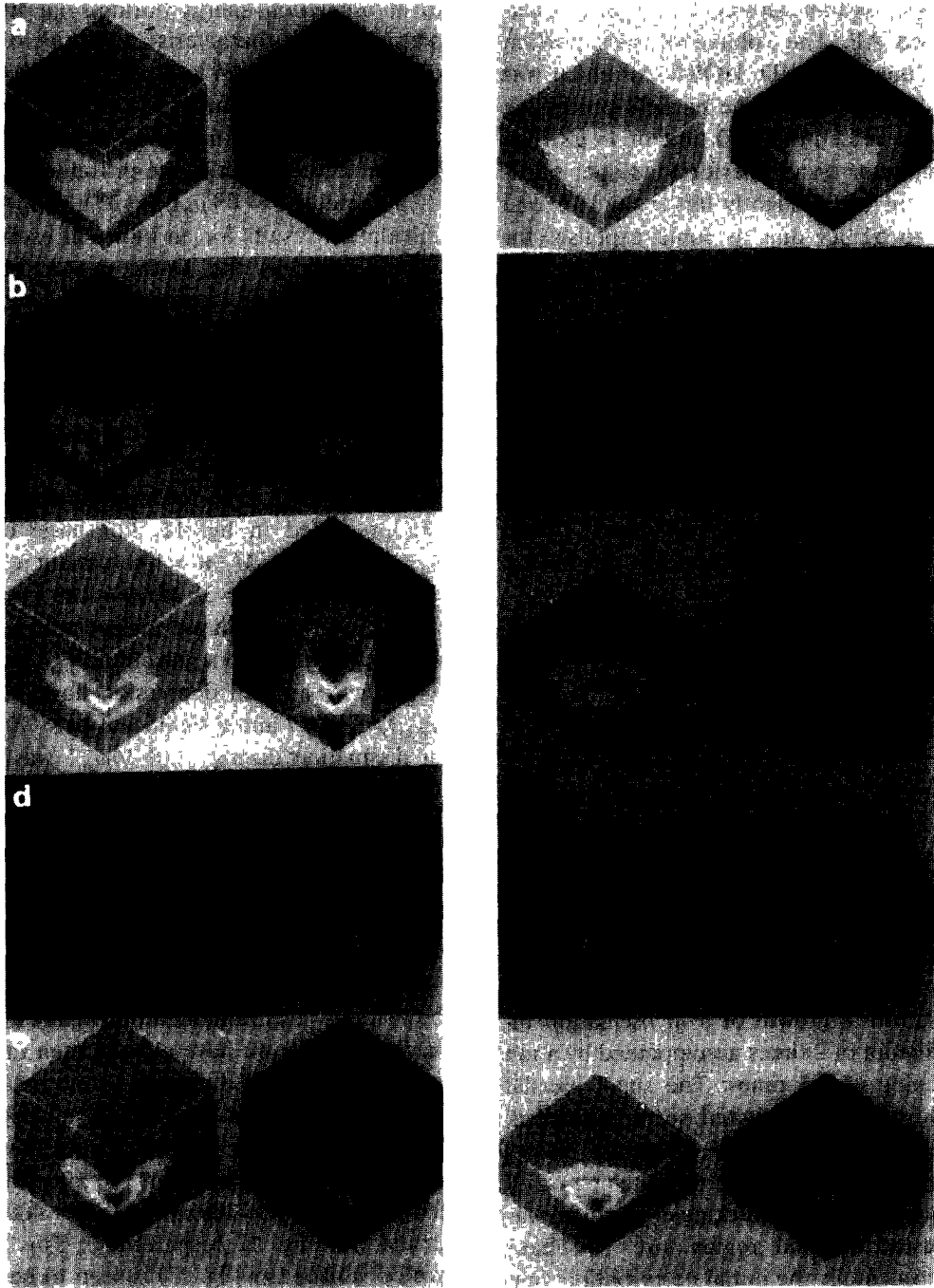


Fig 10 Spatial distributions of hf field energy density  $E^2/8\pi n_0 T_e$  (left) and the ion density  $n_i/n_0$  (right) for variant  $\rho_0 = 0.015$ ,  $M/m = 400$  (a) for  $t = 0$ , (b) the intensive hf field growth stage ( $t = 70.4 \omega_p^{-1}$ ), (c) the time of hf field maximum in the cavity ( $t = 139.2 \omega_p^{-1}$ ), (d) the stage of hf field burning-out ( $t = 210.4 \omega_p^{-1}$ ), (e) the time of the maximum cavity depth ( $t = 284.0 \omega_p^{-1}$ ) (Left side) the whole region, (right side) the cross-section by plane  $z = 0$

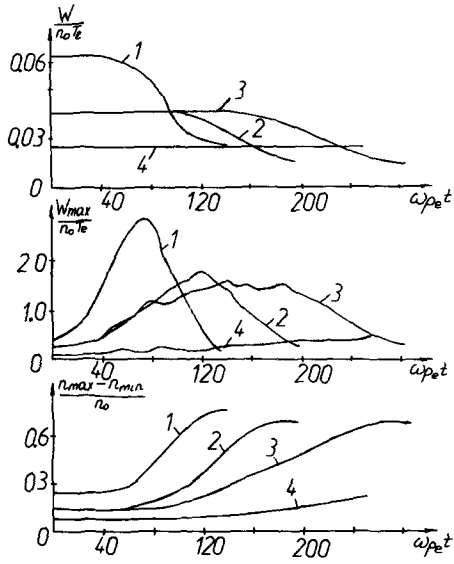


Fig 11 Temporal dependencies of collapsing cavity characteristics (1)  $\rho_0 = 0.020$ ,  $M/m = 100$ , (2)  $\rho_0 = 0.015$ ,  $M/m = 100$ , (3)  $\rho_0 = 0.015$ ,  $M/m = 400$ , (4)  $\rho_0 = 0.010$ ,  $M/m = 100$  (a) The average hf field energy  $W/n_0 T_c$  in the cavity, (b) maximum hf field energy in the cavity, (c) maximum value over space of cavity depth  $(n_{max} - n_{min})/n_0$

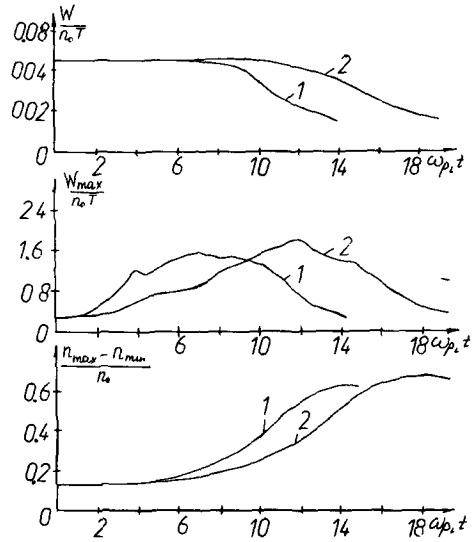


Fig 12 The same as in fig 11 on ion time-scale for variants (1)  $\rho_0 = 0.015$ ,  $M/m = 400$ , (2)  $\rho_0 = 0.015$ ,  $M/m = 100$

tia role in the 3D case for the bright collapse variants the main ion density well depression was after the hf field reached its maximum (see fig. 11). The hf energy levels and plasma density variation values reached exceeded appreciably (more than twice) the observed ones in analogous 2D calculations.

The field and density variation spatial dependences along and perpendicular to the dipole axis presented in figs. 13 and 14 for variant  $\rho_0 = 0.15$ ,  $\epsilon = 3$ ,  $M/m = 400$  for the time moments  $t_1 = 0$ ,  $t_2 = 139.2\omega_p^{-1}$  (at which the field is at its maximum) and  $t_3 = 284\omega_p^{-1}$  (at which the density deformation is at its maximum). The cavity eccentricity (the long size to small size ratio) at the time moments  $t_1, t_2, t_3$  was 1.65, 2.1, 2.3 for the field intensity and 1.65, 2.3, 2.2 for the density well, i.e. during the evolution the cavity preserved the dipole flattened shape tending to a more spatial anisotropic shape.

One of the most important simulation results which we have observed for all bright collapse

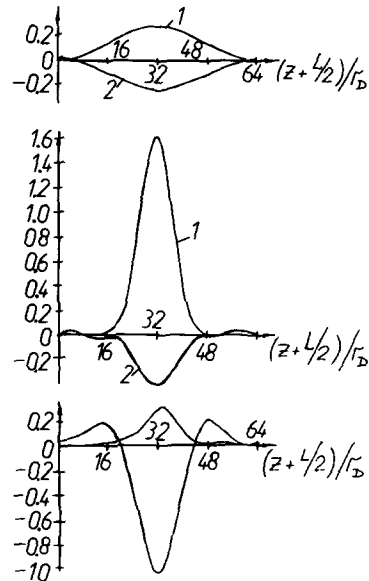


Fig 13 Distributions along the dipole axis of values  $E^2/8\pi n_0 T_c$  (curves 1) and  $2\delta n/n_0$  (curve 2) for variant  $\rho_0 = 0.015$ ,  $M/m = 400$  (a)  $t = 0$ , (b)  $t = 139.2\omega_p^{-1}$ , (c)  $t = 284.0\omega_p^{-1}$

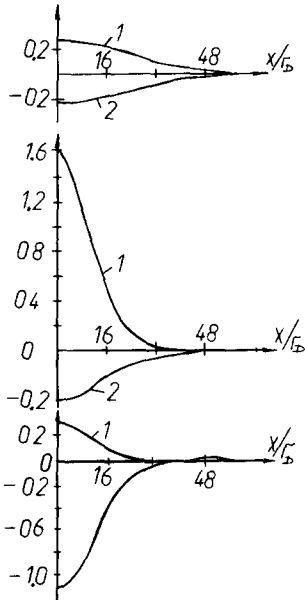


Fig 14 The same as in fig 13 perpendicular to the dipole axis

variants is the rather large ( $\sim 10r_D - 16r_D$ ) minimal cavity size; in the 2D case this value was  $\sim 10r_D$ . This result is in good agreement with laboratory experiments [2] (see also ref. [3]) which seemed previously inexplicable. The explanation could be in the fact that because of a higher value of  $W_{\max}/n_0T_e$  than in the 3D case the electron-oscillation interaction is appreciably modified by the strong nonlinearity. This assumption is confirmed by the phase plane picture ( $z, V_z$ ) analysis (see fig. 15,  $z$  is the field oscillation direction, the picture is averaged in perpendicular direction). The “curls” formation is clearly seen, i.e. wavebreaking takes place. The final electron velocity distribution (see fig. 16) is characterized by a substantial anisotropy (the maximum electron acceleration along the dipole axis) and the existence of strongly accelerated, up to  $V = V_{\max} \approx 9V_{Te}$ , electrons (in 2D calculations  $V_{\max} \approx 5V_{Te}$ , see fig. 5) It means, in particular, that collapse is a more effective mechanism of fast electron generation than one could expect from 2D model calculations.

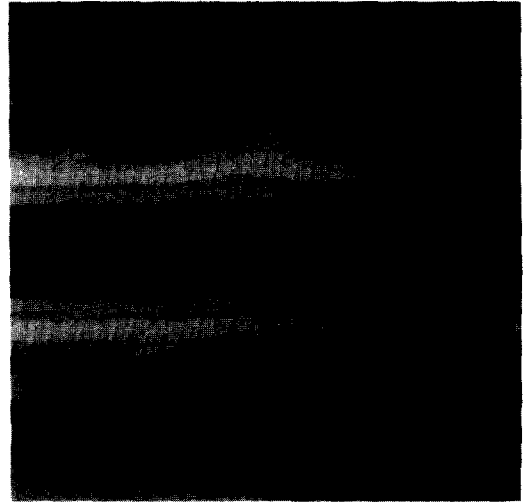


Fig 15 Electron phase plane ( $z, V_z$ ) (in perpendicular direction the picture is averaged) for variant  $M/m = 400, \rho = 0.015$  at the time  $t = 284\omega_p^{-1}$

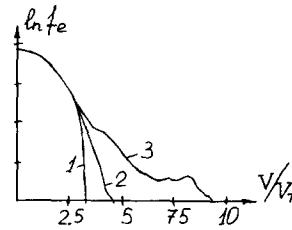


Fig 16 The electron distribution function integrated over space and velocities (1)  $V_x, V_y(t = 0)$ , (2)  $V_x, V_z(t = 284\omega_p^{-1})$ , (3)  $V_x, V_y(t = 284\omega_p^{-1})$  for variant  $\rho_0 = 0.015, M/m = 400$

The number of electrons whose velocities exceed 3, 5 and 7  $V_{Te}$  in dependence on time are presented in fig. 17. The hf oscillation energy is seen to be transformed to a small part of the electrons (about 0.3% of the total number) belonging to the tail of the distribution function. The growth of accelerated particles starts when the hf field is maximal. This fact demonstrates that the collapse is stopped simultaneously with the beginning of the effective electron acceleration.

The results obtained in the 3D kinetic simulation – the local level of high hf oscillation, the quasi-one-dimensional electron distribution function tail, the flattened cavity shape – allow us

to use for a qualitative general physical picture analysis in the final stage the auxiliary one-dimensional particle-method simulation of high-intensity hf energy structures over the ion density well. One should note that 1D kinetic calculations of large-amplitude wave evolution were carried out, for example, in works of Buchel'nikova and co-workers (see, e.g., ref [34]) In contrast to these works we have investigated the dissipation distribution process obtained as a 3D evolution result. For the sake of simplicity we have carried out auxiliary 1D calculations for periodical boundary conditions, i.e. two full cavities with oppositely directed electric fields were considered.

The field structure in the cavities was simulated by a soliton-type initial distribution

$$E(x) = E_0 \left[ 1/\text{ch } \lambda(x - L/4) - 1/\text{ch } \lambda(x - 3L/4) \right],$$

where  $L$  is the region size, for parameters ( $E_0$  the amplitude,  $\lambda$  the inverse size) corresponding to 3D cavity parameters at the beginning time of field burning out. The ion density deformation value was defined from hf and kinetic pressures balance,

$$\alpha \frac{E^2}{16\pi n_0 T_e} = -\frac{\delta n}{n_c} + C,$$

$$C = \frac{1}{16\pi n_0 T_e L} \int_0^L E^2 dx,$$

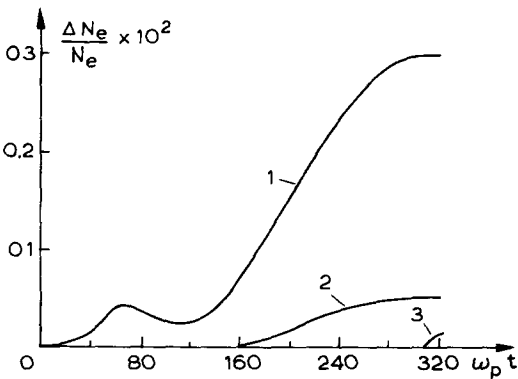


Fig 17 Temporal dependencies of the number of electrons whose velocities exceed (1)  $3V_{Te}$ , (2)  $5V_{Te}$ , (3)  $7V_{Te}$  for variant  $\rho_0 = 0.015$ ,  $M/m = 400$

where  $\alpha$  is the coefficient which allows to calculate the required field using the known field amplitude

Using the above initial distribution for cavity parameters  $W_{\max}/n_0 T_e = 1.8$ ,  $-\delta n/n_0 \sim 0.5$  and cavity half-width  $15r_D$  corresponding to the 3D variant  $\rho_0 = 0.015$ ,  $\epsilon = 3$ ,  $M/m = 400$ , we have observed a fast (2–3 plasma periods) burning out of such structure accompanied by a formation of a tail in the accelerated particle electron distribution function; the ion cavity profile during this time remained practically unchanged (see fig 18).

From the phase space picture corresponding to this variant the peculiarity formation with subsequent transformation into multiflow is clearly seen (fig 19). The zero electron temperature and with the same initial conditions calculation variant (the phase space plane evolution presented in fig. 20) gave a more clear multiflow picture origin

The physical interpretation of the energy transformation to electrons is studied next. The cavity electric field changes its direction during the time  $\tau \sim \pi/\omega_p$ . If a sufficient number of electrons succeed in crossing the whole cavity during this time then a substantial part of the trapped energy is taken away by these particles from the cavity. The oscillations of the electric field in our calculations are so large that even initially immobile particles succeed in accelerating and leave the cavity within the time  $\tau$ . In this process a part of the particles is reflected back and produces multiflow motion, which is clearly observed in fig 19. The finite temperature washes away the picture but the main phase space structures are observed sufficiently well

For 3D simulation a similar phase space behavior is also revealed. The absence of a break in the small-velocity region is explained by the fact that the picture given in fig 15 is averaged in perpendicular direction and particles from the cavity periphery, where the field is negligible, fill the break. One should note also that the part of burned energy in 1D calculations is about 80%, which is in good agreement with 70% of the burned-out energy in 3D simulation

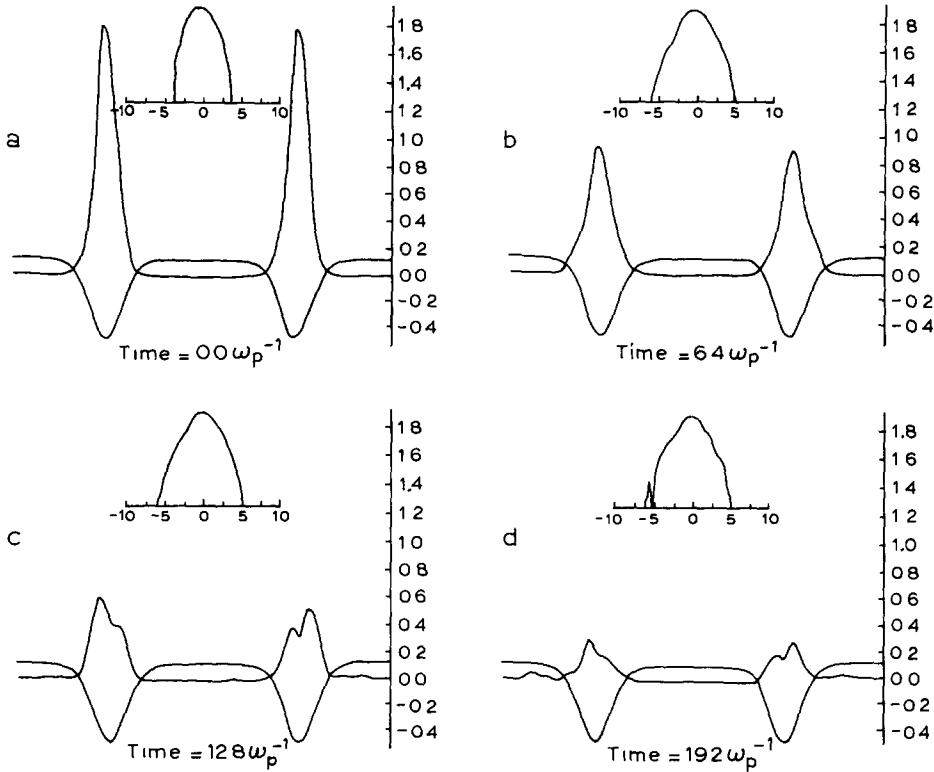


Fig 18 Spatial distributions of hf field energy density  $E^2/8\pi n_0 T_e$  and the plasma density variation  $\delta n/n_0$  and also the electron distribution function (top) in the 1D experiment (a)  $t = 0$ , (b)  $t = 6.4 \omega_p^{-1}$ , (c)  $t = 12.8 \omega_p^{-1}$ , (d)  $t = 19.2 \omega_p^{-1}$

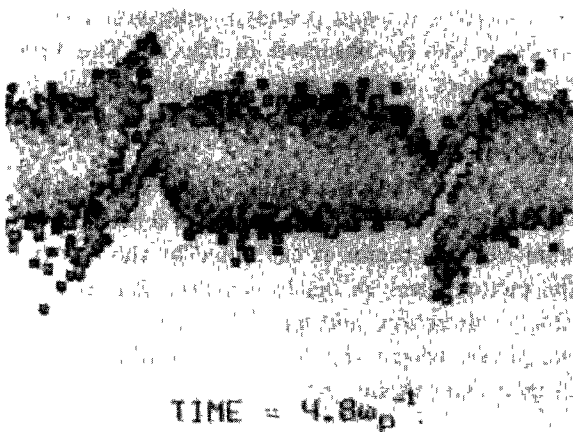


Fig 19 Electron phase plane for a time  $t = 4.8 \omega_p^{-1}$  in the 1D experiment

The initial cavity size increase decreases substantially the energy transmission to particles. The hf field level decrease in the cavity acts similarly. To simulate such an effect we shall take into account that in the real 3D situation the cavity collapse preserves the plasmon number  $N \sim W_{\max} l^3$ , where  $l$  is the characteristic size,  $W_{\max}$  the maximum value of the hf energy in the cavity. Therefore the sizes  $r_1$  and  $r_2$  corresponding to  $W_{1\max}$  and  $W_{2\max}$  are connected by  $r_2 = r_1 W_{1\max} / W_{2\max}$ . This allows us to simulate the cavity dissipation described above in the more recent stage. The value  $W_{\max}/n_0 T_e = 0.5$  for the above described example  $W_{\max}/n_0 T_e = 1.8$ ,  $r_2 =$

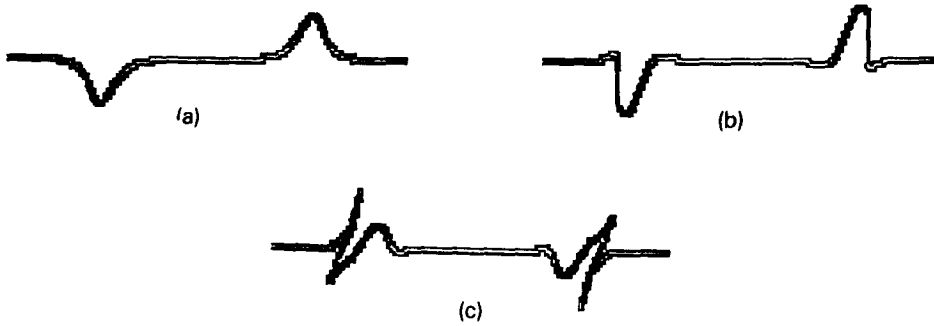


Fig. 20 The phase plane evolution in the 1D experiment for  $T_e = 0$  (a) initial stage ( $t = 1.2 \omega_p^{-1}$ ), (b) wave breaking ( $t = 3.2 \omega_p^{-1}$ ), (c) the multiflow ( $t = 6.0 \omega_p^{-1}$ )

$15r_D$  corresponds to the length  $r = 24r_D$ . The variant of the calculation with the initial condition  $W_{\max}/n_0T_e = 0.5$ ,  $r_2 = 24r_D$  has demonstrated a practically unchanged energy value localized in the cavity during several plasma periods. This fact emphasizes the threshold character of the hf energy burning-out process in dependence on field amplitude and its localization size.

Thus, the investigation of the 3D cavity evolution final stage has demonstrated a clear collapse picture. The general characteristics of the cavity and its interaction with electrons – the maximum hf energy levels, the ion density deformation amplitude, the maximum electrons velocity, the minimum final cavity size – exceed substantially the analogous characteristics in the 2D kinetic calculations. The geometrical cavity characteristics – the large minimum size ( $\sim 16r_D$ ) and anisotropy power – agree with experimentally observed ones [2, 3]. The burning out of high intensive structures is accompanied by formation of phase-space vortices, generation of multiflow and a throwing out of a substantial part of the particles from the cavity.

One should note that stable registration of a sufficiently large minimum cavity size means, in particular, that one of the most important cavity parameters – trapped oscillations characteristic wave number – remains small ( $kr_D \sim 0.2$ ) up to the final stage of evolution. This fact can play an appreciable role for a simplified description of

building up of the collapse. On the other hand, a large minimum cavity size can lead to the fact that the inertial interval length for real plasma experiments will not be very large. This fact must be taken into account in the interpretation of experimental results.

One should emphasize finally the following. As calculation results show [32, 33] the density fluctuations excited by the ponderomotive forces during the cavity collapse can affect substantially the turbulence properties. In several works (see ref [33] and references therein) attention was paid to the “nucleation” of the collapsing cavities, i.e. the rise of cavities on the location of the burned-out ones. This effect depends substantially on the well density structure at the location of the burned-out cavity. In ref. [33] the 2D simulation in the framework of the dynamical equations was carried out. Our calculations show that the maximum density fluctuation amplitude which is reached already after the cavity burning on the inertial compression stage even in the 2D case is large,  $\delta n/n_0 \sim 0.3-0.4$ . In 3D calculations this value is increased up to  $\delta n/n_0 = 0.7$ . Kinetic effects are already very important for such fluctuations and this fact must be taken into account in carrying out turbulence simulation. In particular, the problem of the level and the fluctuation spectrum remaining after the cavity burning-out have to be studied using the particle method. It is convenient to do this using the semi-kinetic model (25)–(27) described in section 3.

## 7. Conclusions

We have carried out a Langmuir collapse numerical simulation which includes the physical picture analysis of the especially important cavity evolution final stage. Such an investigation based on 2D and 3D kinetic calculations became possible due to especially designed and practically realized general principles of the Langmuir collapse simulation. These principles are based on rigorously taking into account of the cavity physics in the model, through co-ordinated performance of all problem stages – from physical statement to software development.

The 2D problem solution in the wide inertial interval (“through simulation”) have demonstrated the collapse of cavities which trapped a large energy amount and quasistationary cavitons for low exceedings. This result must be taken into account in the interpretation of 2D turbulence simulation results and their extrapolation in the 3D case.

The 3D particle simulation has demonstrated a clear collapse and particle acceleration picture Agreement between the cavity characteristics with ones observed in laboratory experiments has been obtained The calculation results point out the important role of joint nonlinear and kinetic effects taken into account in theoretical models of turbulence and present useful data for building-up of such models and interpretation of the experiments

## References

- [1] V E Zakharov, *Sov Phys JETP* 35 (1972) 908
- [2] A Y Wong and P Y Cheung, *Phys Rev Lett* 52 (1984) 1222, *Phys Fluids* 28 (1985) 1538
- [3] D M Karfidov, A M Rubenchik, K F Sergeichev and I A Sychev, to be published
- [4] V E Zakharov, in *Basic Plasma Physics*, Vol 2 (Elsevier, Amsterdam, 1985), p 81
- [5] V D Shapiro and V I Shevchenko, in *Basic Plasma Physics*, Vol 2 (Elsevier, Amsterdam, 1985), p 123
- [6] M V Goldman, *Rev Mod Phys* 56 (1984) 709
- [7] A M Rubenchik, R Z Sagdeev and V E Zakharov, *Comm Plasma Phys Contr Fus* 9 (1985) 183
- [8] S I Anisimov, M A Beresovski, V E Zakharov, I V Petrov and A M Rubenchik, *Sov Phys JETP* 57 (1983) 1192
- [9] L M Degtyarev, V E Zakharov, R Z Sagdeev, G I Soloviev, V D Shapiro and V I Shevchenko, *ZhETF* 85 (1983) 1221 [in Russian]
- [10] M A Mal'kov, R Z Sagdeev, V D Shapiro and V I Shevchenko, in *Nonlin and Turb Proc in Phys* (Harwood, New York, 1983) p 405
- [11] V M Malkin, *ZhETF* 87 (1984) 433, 90 (1986) 59 [in Russian].
- [12] M B Isichenko and V V Yan'kov, *Fiz Plasmy* 12 (1986) 169 [in Russian]
- [13] A I D'yachenko, V E Zakharov, A M Rubenchik, R Z Sagdeev and V F Shvets, *JETP Lett* 44 (1986) 648
- [14] V L Galinski, M A Mal'kov and G I Soloviev, *Fiz Plasmy* 13 (1987) 1269 [in Russian]
- [15] P A Robinson, D L Newman and M V Goldman, *Phys Rev Lett* 61 (1988) 702, 62 (1989) 2132
- [16] A I D'yachenko, V E Zakharov, A M Rubenchik, R Z Sagdeev and V F Shvets, *Sov Phys JETP* 67 (1988) 513
- [17] V E Zakharov, A N Pushkarev, A M Rubenchik, R Z Sagdeev and V F Shvets, *JETP Lett* 47 (1988) 287
- [18] V E Zakharov, A N Pushkarev, A M Rubenchik, R Z Sagdeev and V F Shvets, *ZhETF* 96 (1989) [in Russian]
- [19] V E Zakharov *Usp Fiz Nauk* 155 (1988) 529 [in Russian]
- [20] L M Degtyarev and V E Zakharov, preprint IPM AN SSSR No 106 (1974) [in Russian]
- [21] A Yu Golovin, A N Pushkarev, R Z Sagdeev, V F Shvets and V I Shevchenko, Preprint IKI AN SSSR No 1347 (1988) [in Russian]
- [22] A I Dyachenko, A N Pushkarev, A M Rubenchik and V F Shvets, *Comput Phys Commun*, 60 (1990) 239
- [23] R W Hockney and J W Eastwood, *Computer Simulation Using Particles* (McGraw-Hill, New York, 1981)
- [24] C K Birdsall and A B Langdon, *Plasma Physics via Computer Simulation* (McGraw-Hill, New York, 1985)
- [25] M A Beresovski, M F Ivanov, I V Petrov and V F Shvets, *Programmirovanie* 6 (1980) 37 [in Russian]
- [26] V E Zakharov, A N Pushkarev, R Z Sagdeev, G I Soloviev, V D Shapiro, V F Shvets and V I Shevchenko, *Dokl AN SSSR* 305 (1989) 598 [in Russian]
- [27] A N Poludov, R Z Sagdeev and Yu S Sigov, preprint IPM AN SSSR No 128 (1974) [in Russian]
- [28] A N Poludov, B D Selandin and Yu S Sigov, *Dokl AN SSSR* 246 (1979) 58 [in Russian]
- [29] T Tajima, M V Goldman, J N Lebouef and J M Dawson, *Phys Fluids* 24 (1981) 182
- [30] S I Anisimov, M A Beresovski, M F Ivanov, I V Petrov, A M Rubenchik and V E Zakharov, *Phys Lett A* 92 (1982) 32
- [31] M Yu Baryshev and A D Yunakovski, preprint IPF AN SSSR No 105 (1984) [in Russian]
- [32] L M Degtyarev, R Z Sagdeev, G I Soloviev, V D Shapiro and V I Shevchenko, *ZhETF* 95 (1989) 1690 [in Russian]
- [33] D Russel, D F DuBois and H A Rose, *Phys Rev Lett* 60 (1988) 581
- [34] N S Buchelnikova and E P Matochkin, Preprint IYaF SO AN SSSR No 155 (1986) [in Russian]